# Developing a magnetic nanocomposite adsorbent based on carbon quantum dots prepared from Pomegranate peel for the removal of Pb(II) and Cd(II) ions from aqueous solution

**Hamideh Asadollahzadeh[a,*], Mahdiyeh Ghazizadeh[a] and Mohammad Manzari[a]**
*[a]Department of Chemistry, Faculty of Science, Kerman branch,*
*Islamic Azad University, Kerman, Iran, P. O. Box 7635131167, Kerman, Iran*

**ABSTRACT**

Agriculture waste is a good choice for the production of carbon dots owing to its abundance, wide availability, eco-friendly nature. In this study a novel magnetic bioadsorbent based on carbon quantum dots ($Fe_3O_4$-PPCQDs) from Pomegranate peel (PP) was used as adsorbent to remove lead (Pb) and cadmium (Cd) from 50 mL of water and wastewater samples by magnetic solid phase extraction (MSPE). After adsorption ions with $Fe_3O_4$-PPCQDs at pH=6, the concentration of Pb(II) and Cd (II) ions were determined by flame atomic absorption spectrometry (F-AAS). The manufactured of $Fe_3O_4$-PPCQDs and GO nanostructures were structurally characterized by scanning electron microscopy (SEM), transmission electron microscopy (TEM), X-ray diffraction (XRD) and Fourier transform infrared spectroscopy (FT-IR). The quantum dots were optically characterized by UV–Vis spectroscopy. Batch adsorption experiment was conducted to examine the effects of pH, contact time, temperature and initial concentration of Pb(II) and Cd(II) from the water. The preconcentration factor and LOD for Cd and Pb were obtained 50 and (1.3 μg L$^{-1}$; 15.5 μg L$^{-1}$), respectively. The equilibrium data of ions sorption were well described by Langmuir and Freundlich model. The $R^2$ values obtained by Langmuir model were higher. The absorption capacity of $Fe_3O_4$-PPCQDs for cadmium and lead were obtained 17.92 and 23.75 mg g$^{-1}$, respectively.

## 1. Introduction

Environmental pollution based on the organic chemical compounds (VOCs) and heavy metals (M) have needed a serious threat due to the rapid development of the chemical industry and the toxic effect in environment. The contamination of heavy metals in water through the industrial wastewater is the global environmental problems [1]. The heavy metals compounds cannot be decomposed naturally and cause the various health problems in the living organism and human. Recently, the elimination of heavy metals is becoming a significant concern as a result of their persistence into the atmosphere [2]. Among of heavy metals, cadmium and lead (Cd and Pb) can be discharged from the several industrial effluents. Cadmium is liberated into the environment from the steel production, the cement manufacture, the Ni-Cd battery manufacture, cadmium electroplating, the phosphate fertilizers etc. [3]. Bivalent cadmium causes a number of deformities and diseases in humans, such as the muscle cramps, the lung problems, the

*Corresponding Author: Hamideh Asadollahzadeh
Email: asadollahzadeh90@yahoo.com

kidney degradation, the proteinuria, the skeletal deformation [4]. On the other hand, common anthropogenic causes of lead contamination in groundwater include the smelting, the mining, the consumption of fossil fuels and the incinerating solid waste [5]. Lead can cause a cognitive dysfunction in children, high blood pressure, the illnesses of the immune system and the reproductive system [6]. Numerous techniques have been used to reduce the harmful effects of cadmium and lead on water source, including the chemical oxidation and the reduction, the chemical precipitation, the ion exchange, the electrochemical processes, and the membrane filtration [7]. The performance and perform of above processes are difficult without any selectivity. However, among these methods, the adsorption technique is flexible, low cost and has a high efficient recovery [8]. Adsorption is a mass transfer process where a substance is transferred from the liquid phase to the surface of the solid through physical or chemical interaction. Many kinds of adsorbents, including the activated carbon [9], the inorganic minerals [10], the biomass adsorbents [11-13], and polymer [14–17] are used to remove the metal ions from the liquid phased such as water and wastewater. By-products from agriculture feed have always considered due to its availability and the cost features. Moreover, the other important characteristics are biocompatibility, biodegradability and the renewable [18]. Thus there is an interest in use of agricultural wastes as a source for preparation of carbon based nanomaterial. Carbon based quantum dots are new class of carbon nanomaterials that have been explored due to their excellent properties [19].

However, the separation of adsorbents, obtained from agricultural waste, required a high-speed centrifugation or filter due to they are too small [20]. Iron oxide has excellent magnetic properties, the high biocompatibility, easy separation through external magnetic field, reusability and comparatively low cost. The magnetic iron oxide was fixed inside the polymer adsorbent matrix with the highest adsorption rates [21]. The surface modification of the activated carbon-based iron oxide using the coating technique improves their sorption capacity because, the surface coating phenomenon helps to converting the closely - packed cubic geometry of magnetic nanoparticles into compact [22].

Pomegranate peel (PP), as a by-product of the pomegranate juice industry is an inexpensive material. It is composed of several constituents, including polyphenols, ellagic tannin and ellagic acids [23]. So far, no study has been done on surface modification of iron oxide by using carbon quantum dots prepared from pomegranate peel for developing magnetic nanocomposite ($Fe_3O_4$-PPCQDs). The PPCQDs adsorbent has generated from the pomegranate peel and functionalized with $Fe_3O_4$ as magnetic nanostructure which was used for removing toxic ions from wastewater. Another advantage is that the loaded adsorbents could be easily separated from the aqueous solution using magnet instead of centrifugation thus conserving energy. In this study, the material preparation, the characterization and the batch-type removal experiments were carried out wherein the feasibility of the above described composite for the removal of heavy metals Cd(II) and Pb(II) from aqueous solution which were investigated by varying the process conditions.

## 2. Material and Methods
### 2.1. Apparatus
The concentration of heavy metals (Pb and Cd) in the aqueous solution was measured using flame atomic absorption spectrometry (F-AAS, Model AAnalyst 800, Air acetylene, Perkin Elmer, USA). The wavelength of 217.0 nm (Slit :1, Current lamp: 5mA) and 228.8 nm (Slit: 0.5, Current lamp: 3 mA) was used for lead and cadmium determination, respectively. The working ranges for lead and cadmium were achieved 2.5-20 mg L$^{-1}$ and 0.2-1.8 mg L$^{-1}$, respectively by sensitivity of 0.06 mg L$^{-1}$. The LOD of F-AAS for lead and cadmium was achieved 0.1 mg L$^{-1}$ and 0.05 mg L$^{-1}$, respectively. The auto-sampler from 0.5 to 5 mL was used for sample introduction to F-AAS. The pH was measured by electronic pH meter (Benchtop meter inoLab pH 7110 model, WTW company, Germany).

## 2.2. Chemicals

Pomegranate peel were obtained from Mahan, Kerman, Iran. Sodium hydroxide (NaOH), cadmium nitrate tetrahydrate ($Cd(NO_3)_2 \cdot 4H_2O$), lead nitrate ($Pb(NO_3)_2$), the ferric chloride hexahydrate ($FeCl_3 \cdot 6H_2O$), the ferric sulfate heptahydrate ($FeSO_4 \cdot 7H_2O$) hydrochloric acid (HCl) with a purity of 37%, nitric acid ($HNO_3$) with purity 63% was purchased from Merck and all the chemical reagents were analytical grade. All the aqueous solutions were prepared by using double distilled water. The pH of the solution was adjusted and measured using electronic pH meter. The pH of the solution was adjusted by adding 0. 1M HCl or 0. 1M NaOH and measured using electronic pH meter (Benchtop meter inoLab pH 7110 model, WTW company, Germany).

## 2.3. Synthesis of Magnetic Carbon Quantum Dots (Fe₃O₄-CQDs)

The pomegranate peel (PP) has carbon structure which was ground after washed/ dried in the oven 100°C. The ground powder is sifted by small mesh to obtained for used for synthesis of CQDs. First of all, 100 grams of ground powder of the pomegranate peel (PP) mixed with 8 Liters of DW in the 500 mL closed container. The closed container adjusted on temperature between 200-230°C for two days and then the temperature decreased (cooling) up to room temperature for one day. The sediments were separated in by Watman filter paper based on the vacuum pump and the black brown product is created. After UV irradiation (400 nm), the color of product change into blue photoluminescence which was showed that a quantum dot particles synthesized correctly. The CQDs cab be absorbed the UV irradiation at 220 nm spectrophotometer. The final liquid product filtered / dried completely at temperature of 100 °C and finally converted into powder. The powder put in the oven based on quartz type, $N_2$ gas and 700 °C (1 hour). Then the product powder was carbonized and impurities get out of oven. After synthesis PPCQDs, the absorption of UV was obtained at 210 nm which was confirmed by UV peak by spectrophotometer (Fig.1a). the

magnetic Fe₃O₄-PPCQDs were prepared by co-precipitation of $FeCl_2 \cdot 4H_2O$ and $FeCl_3 \cdot 6H_2O$, in the presence of PPCQDs [24]. To prepare the nano magnetic PPCQDs, 10 mg of PPCQDs in 10 mL of DW was ultra-sonicated for I h. To the resulting mixture was added 12.5 mL solution of $FeCl_2 \cdot 4H_2O$ (125 mg) and $FeCl_3 \cdot 6H_2O$ (200 mg) in deionized water (10 mL) at room temperature. Then, 30% ammonia solution was added for the pH = 11 and the temperature was increased to 60 ˚C. After being stirred for 1 h, the product was cooled at 25°C. finally, the black powder of Fe₃O₄-PPCQDs centrifuged at 4000 rpm for 20 min, washed and dried at 75°C (Fig.1 b).
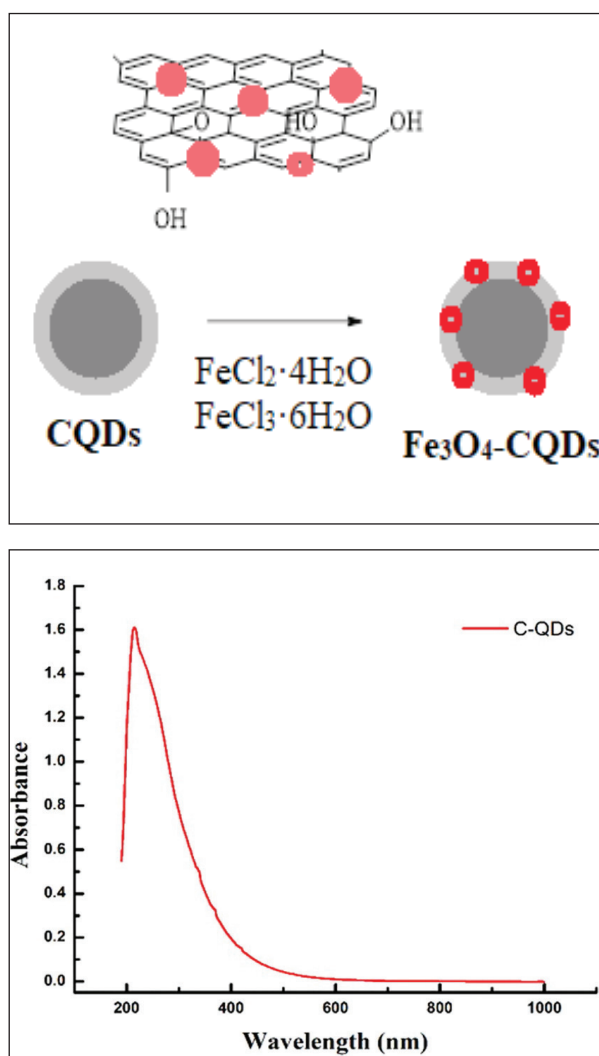




**Fig.1.** a) UV absorption by CQDs product b) The mechanism of synthesis of Fe₃O₄-PPCQDs

### *2.4. Batch mode adsorption and analytical procedure*

Adsorption of Pb(II) and Cd(II) based on $Fe_3O_4$-PPCQDs adsorbent was achieved in optimized experimental conditions such as pH, the contact time, the amount of adsorbent and temperature. The experiments were carried out in 50 ml Erlenmeyer flasks. Experiment parameters were achieved from pH 2 to 8, the sample volume of 50 mL, the contact time between 2 - 60 minute, the amount of biosorbent from 0.01 to 0.2 g, the temperature between 5-45°C and the concentration of ions 5-150 mg $L^{-1}$. To adjust required The pH of aqueous solution was adjusted with HCl (0.1 M) and NaOH (0.1 M). Finally, the thermodynamic parameters and isotherms were studied. The $Fe_3O_4$-PPCQDs were separated with a magnet using its magnetic field, and the filtrate was kept for the further determination of remaining Pb(II) and Cd(II) in water by F-AAS after back extraction solid phase by 1 mL mixture of $HNO_3$ 0.1 M/DW. Moreover, the linear ranges of MSPE procedure for cadmium and lead based on $Fe_3O_4$-PPCQDs were achieved 4-20 μg $L^{-1}$ and 50-140 μg $L^{-1}$, respectively (RSD%<2.4). So, the trace analysis of lead and cadmium (sub-ppb) can be created by the $Fe_3O_4$-PPCQDs adsorbent. The quantity of adsorbed ion per unit mass of biosorbent was calculated from Equation 1:

$$q_e = (C_0 - C_e) \times V/m \quad (1)$$

where $C_o$ and $C_e$ are the concentrations of Pb(II) and Cd(II) at the beginning and at the end of the adsorption process.

## 3. Result and discussion
### *3.1. Characterization*

X-ray diffraction (XRD) patterns were recorded on a Seifert TT 3000 diffractometer (Ahrensburg, Germany). The specific surface areas and pore volume of the sorbents were calculated by the Brunauer-Emmett-Teller (BET) and Barrett-Joyner-Halenda (BJH) methods, respectively. Scanning electron microscopy (SEM, Phillips, Netherland) was used for surface image of the CQDs The morphology of sorbent was examined by transmission electron microscopy (TEM, Philips, Netherland). The Fourier transform infrared spectrophotometer (FTIR, Bruker GmbH, Germany) using KBr pelleting method was used in the 4000–200 $cm^{-1}$

### *3.2. Fourier-transform infrared spectroscopy (FTIR)*

The FTIR spectra of $Fe_3O_4$-PPCQDs adsorbent are shown in Figure 2. The prime spectrum of FTIR of CQDs is shown in black line as nonactivated form (Fig. 2a) and red line (activated/$HNO_3$) which has different wavenumbers but both of them is similar. In these figures, the peak of 1020 $cm^{-1}$,1200 $cm^{-1}$ ,1250 $cm^{-1}$ belong to C-O bond and the peak of 1381 $cm^{-1}$ shows the formation of C-H bond. Additionally a peak of 1585 $cm^{-1}$ is observed for **C=C** bond and the another peak appeared in
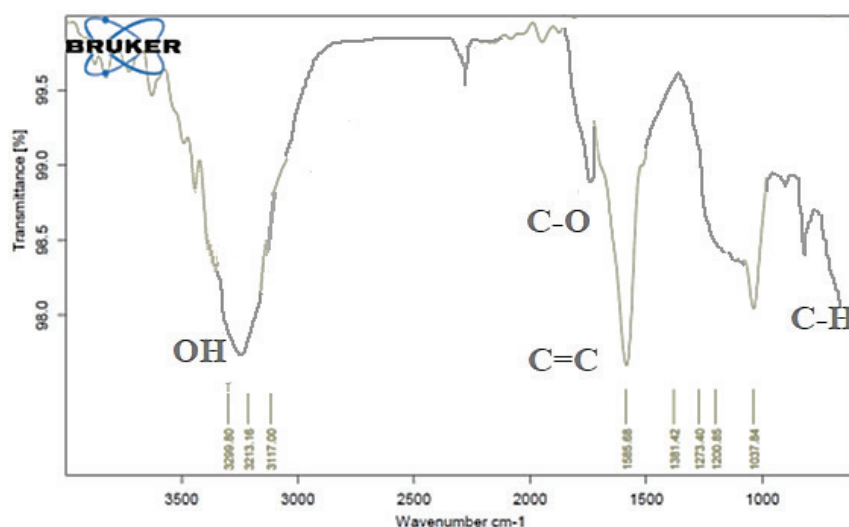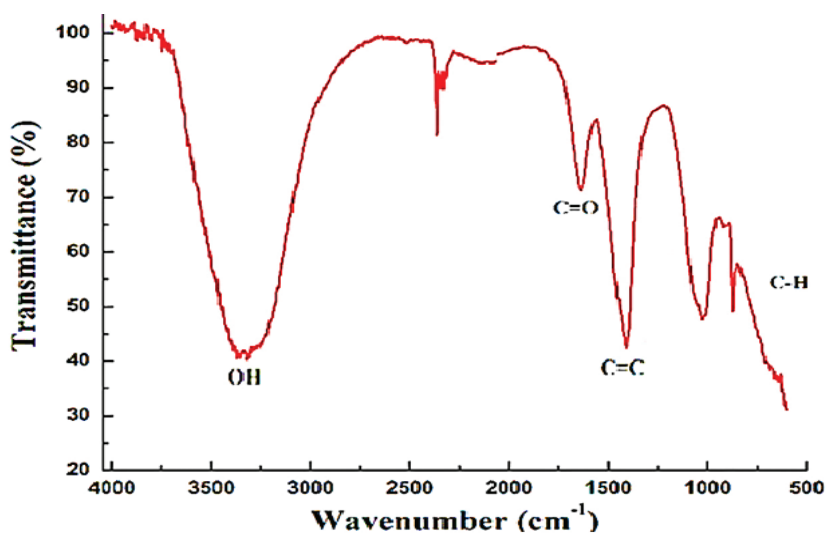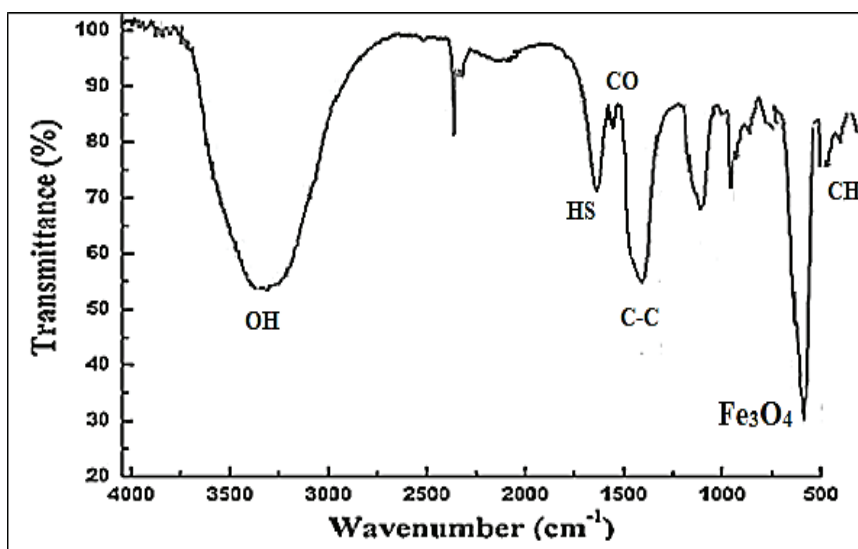


**Fig.2(a).** The spectrum of FTIR of CQDs

**Fig.2(b)**. The spectrum of FTIR of HNO$_3$-CQDs



**Fig.2(c)**. The spectrum of FTIR of Fe$_3$O$_4$-PPCQDs

3300 cm$^{-1}$ shows the O-H bond. In Figure 2 (b), the red graph is the sample activated with nitric acid vapour. Meanwhile similar peaks of 3340 cm$^{-1}$ (O-H bond) were observed in Figure 2(a,b). In addiition FTIR of Fe$_3$O$_4$-PPCQDs was shown in Figure 2 C which has a peak in 582 cm$^{-1}$ belong to Fe$_3$O$_{4.}$

### 3.3. XRD spectra of CQD

In Figure 3, the X-ray diagram was shown for carbon quantum dots(CQDs) and magnetic carbon quantum dots (Fe$_3$O$_4$-PPCQDs). The XRD curve of Fe$_3$O$_4$-PPCQDs is similar to simple

form of CQDs. In this pattern two main Peaks in 2θ is equal to 22-24 degrees and 45 degrees were observed. The observed wide peak is in the intensity of 24 degrees in page (002) relates to the graphite. The width peak can have related to mall size of carbon quantum dots. The observed Fe$_3$O$_4$-PPCQDs peak in 45 degree angle relate to (101) which indicates similar to graphene formed by quantum dot particles. The XRD pattern for CQDs is similar to Fe$_3$O$_4$-PPCQDs which was indicated that carbon quantum dots modified with PP and Fe$_3$O$_4$ did not changed on the structural order of CQDs.
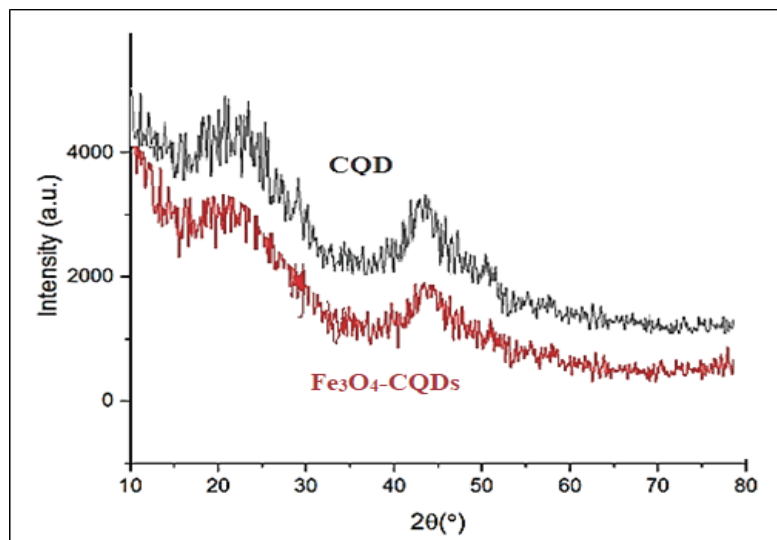
**Fig.3.** The XRD diagram of CQDs and $Fe_3O_4$-PPCQDs

### 3.4. Field emission scanning electron microscope (FE-SEM)

The surface morphology of the CQDs was reported a field emission scanning electron microscope (FE-SEM). The FE-SEM of CQDs have been shown in Figure 4(a). The CQDs primary samples were formed as blocks of nano particles carbon. The blocks are as a colony and forms big volume of CQDs. The smallest size the structure was between 10 to 30 nanometer which consists of very small particles of CQDs. The FE-SEM of the $Fe_3O_4$-PPCQDs was shown in Figure 4(b) with size of 10-25 nm.
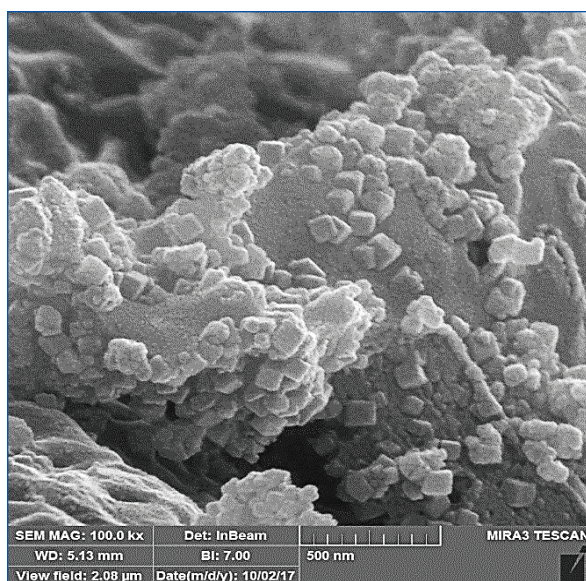
### 3.5. Transmission electron microscopy (TEM)

Transmission electron microscopy (TEM) was used to study of the nanostructure size. The microscopic pictures of the CQDs have been shown in Figure 5a. These pictures are shown clearly a magnified picture which the carbon particles are so small. Moreover, the formation of $Fe_3O_4$-PPCQDs has very small particles which is clearly visible by TEM (Fig.5b).

### 3.6. Bach adsorption studies
### 3.6.1. pH dependent studies

The effect of pH (Fig. 6a and b) on the adsorption of Pb(II) and Cd(II) ions was studied by $Fe_3O_4$-PPCQDs.



**Fig.4a.** The FESEM of CQDs
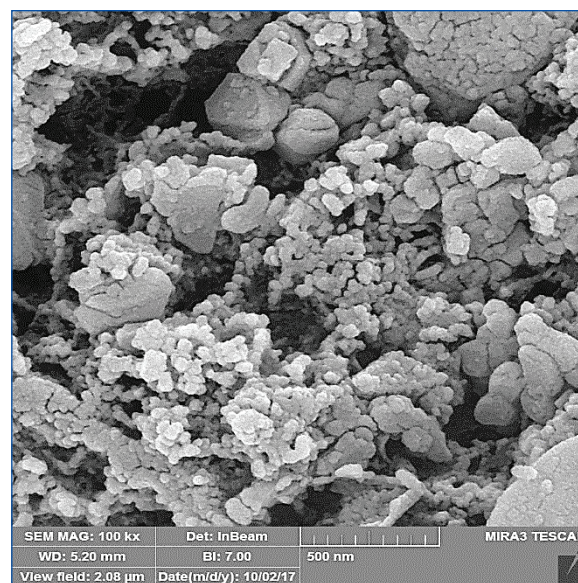


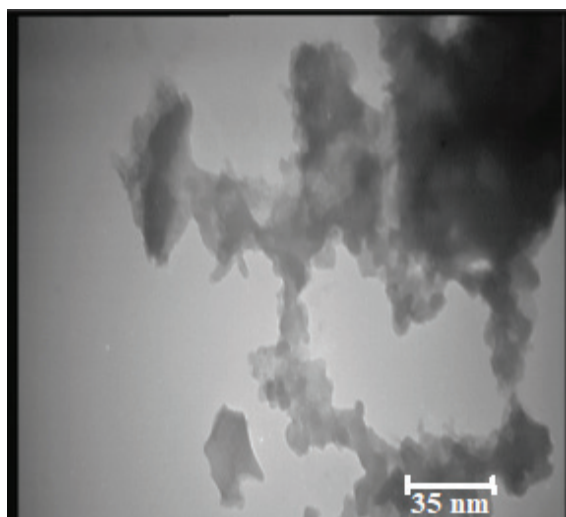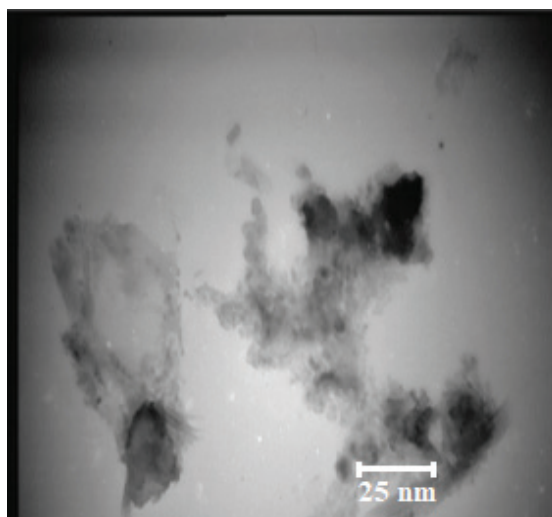**Fig.4b.** The FESEM of $Fe_3O_4$-CQDs

Fig.5a. The TEM of CQDs



Fig.5b. The TEM of Fe$_3$O$_4$-PPCQDs

In order to determine the optimum pH, the pH range between 2.0–11.0 was evaluated for Pb(II) and Cd(II) ions. While screening the pH values, all the other process variables were kept constant. A control experiment was also run (in the absence of Fe$_3$O$_4$-PPCQDs) for the removal Pb(II) and Cd(II) to explore the effect of chemical precipitation (Fig. 6a). The control experiment revealed that there was no removal of Pb(II) and Cd(II) up to pH 7.0 but when the pH was more than 7.0 both ions precipitated as hydroxides [Pb(OH)$_2$ and Cd(OH)$_2$] in the solution thus, leading to their complete removal without Fe$_3$O$_4$-PPCQDs. Also, the adsorption of Fe$_3$O$_4$-PPCQDs was shown in Figure 6b. Due to interaction of ions with adsorbent, the maximum removal for Pb(II) and Cd(II) was achieved at

pH 6.0. The adsorption of Pb(II) and Cd(II) was decreased at lower and upper pH of 6 (5.5>pH>6.5). This behavior may be due to the reason that: lower pH leads to an abundance of hydronium ions (H$_3$O$^+$) in the solution that causes competition between hydronium ions and Pb(II) and Cd(II) ions for adsorption onto Fe$_3$O$_4$-PPCQDs. Thereby lowering the overall adsorption efficiency of these metal ions occurred at lower pH [25]. On the other hand, by increasing pH, the adsorption also increased, which can be showed that in this range (neutral and weakly acidic) most metals are available as soluble and free cations for adsorption. One of the important factors related to the chemical structure of the adsorbent is the point – zero charge pH (pH$_{pzc}$). At this pH, there is no charge on the surface.
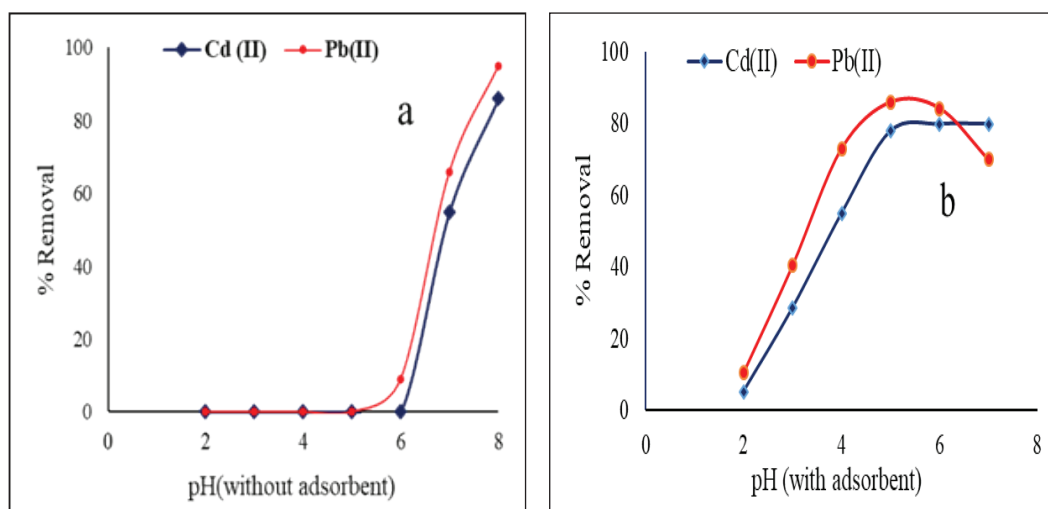


**Fig.6. a)** Effect of pH on Pb(II) and Cd(II) removal without Fe$_3$O$_4$-PPCQDs, **b)** with Fe$_3$O$_4$-PPCQDs adsorbent

### 3.6.2. Effect of time

The effect of contact time on the removal of Pb(II) and Cd(II) by $Fe_3O_4$-PPCQDs was investigated to determine the optimum time taken to attain the equilibrium. The adsorption experiments were carried out by varying the contact time between 2 and 60 min, keeping all other process variables constant. Figure 7 depicts that the removal percentage was increased by increasing of the contact time. The equilibrium was achieved for 20 min and after this time, the further removal for Pb(II) and Cd(II) ions was not observed (constant). It was observed that, the rate of adsorption of ions was faster at initial stages, that this may be attributed to the quick uptake of ions onto the large surface area of $Fe_3O_4$-PPCQDs up to 20 min and after it the adsorption progress was slowly followed and remained constant.
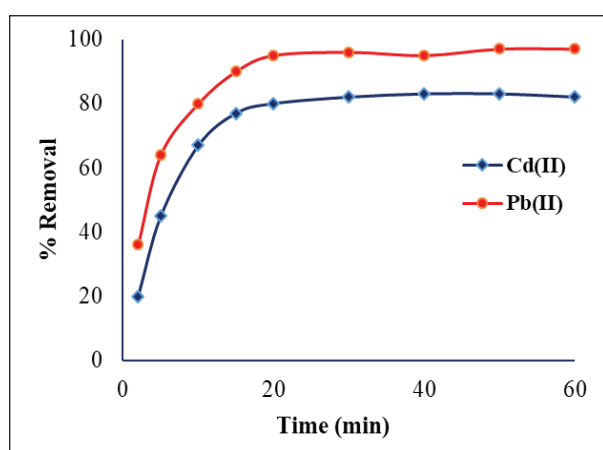


**Fig. 7.** Effect of contact time on Pb(II) and Cd(II) removal by $Fe_3O_4$-PPCQDs

### 3.6.3. Effect of amount of adsorbent

The effect of amount of $Fe_3O_4$-PPCQDs was investigated under optimized conditions (pH=6 and contact time: 20 min.). As shown in Figure 8, the adsorption increased with the $Fe_3O_4$-PPCQDs amount up to 0.1 g. Also, the adsorbent surface has saturated with the extra value of Pb(II) and Cd(II) ions in optimized mass. At higher amount of adsorbent, the adsorption yield is almost unchanged, because the most of Pb(II) and Cd(II) ions interact with $Fe_3O_4$-PPCQDs surface.
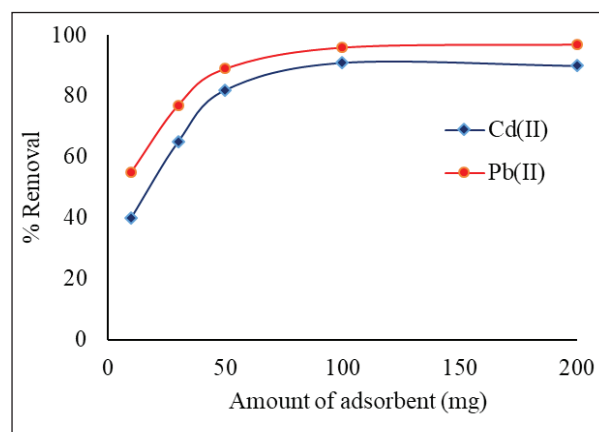


**Fig. 8.** The effect of adsorbent amount on Pb(II) and Cd(II) removal $Fe_3O_4$-PPCQDs

### 3.6.4. Effect of temperature

The effect of the temperature on adsorption of Pb(II) and Cd(II) ions was examined. As shown in Figure 9, the adsorption was reduced as the temperature rising (5 °C–45 °C). The desorption of metal ions on $Fe_3O_4$-PPCQDs was exothermic process and by increasing temperature the removal efficiency decreased. So, the high adsorption of Pb(II) and Cd(II) ions on $Fe_3O_4$-PPCQDs adsorbent depended on the low temperature.
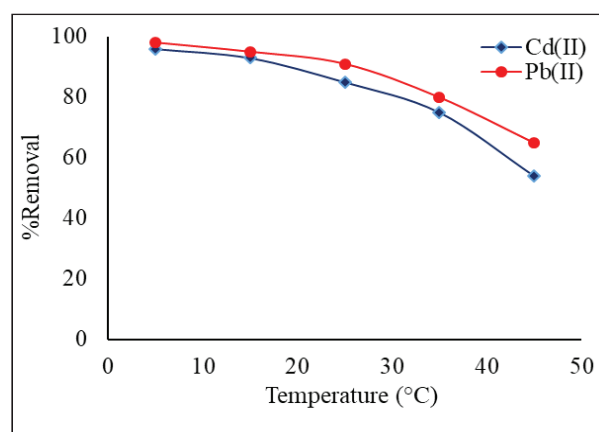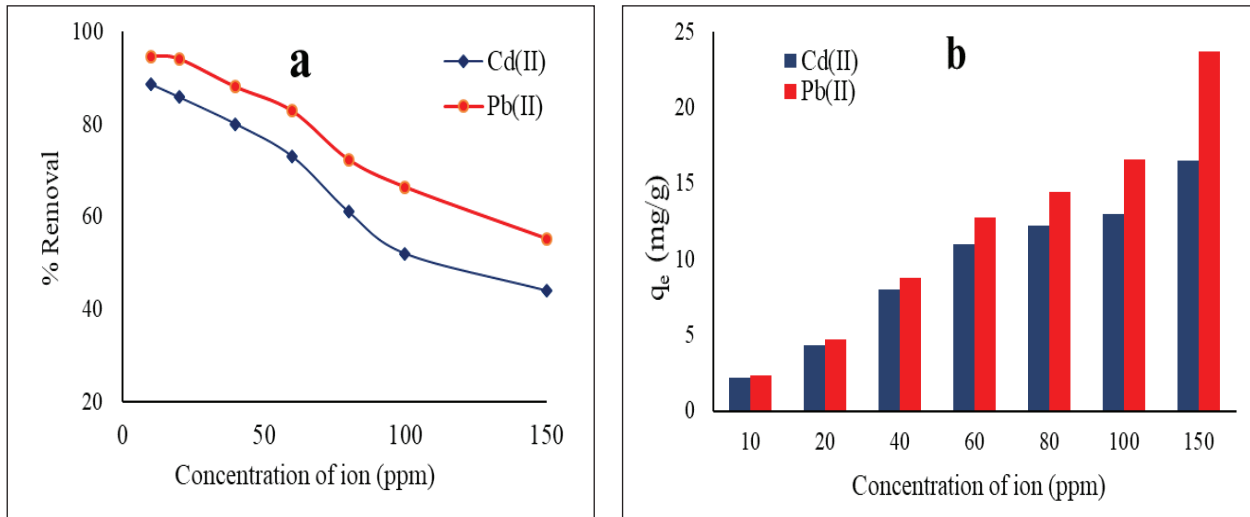


**Fig. 9.** The effect of temperature on Pb(II) and Cd(II) removal by the $Fe_3O_4$-PPCQDs

### 3.6.5. Effect of initial concentration of Cd(II) and Pb(II)

The effect of initial concentrations of Pb(II) and Cd(II) on adsorption process based on $Fe_3O_4$-PPCQDs were evaluated at various concentration from 10 to 150 mg $L^{-1}$. In addition, the all of other parameters are

**Fig. 10. a**). Effect of initial metal ion concentration on Pb(II) and Cd(II) removal by Fe$_3$O$_4$-PPCQDs, **b**) adsorption capacity against metal ion concentration.

constant which is shown in Figure 10a. The Figure 10a revealed that the metal removal was reduced by the Fe$_3$O$_4$-PPCQDs when the metal concentration increased from 10 to 150 mg L$^{-1}$ in the solution. The results showed, the removal efficiencies (%) were decreased for Cd(II) and Pb(II) from 88.60 to 44 and 94.61 to 55.22, respectively. The reduce of removal efficiency (%) by increasing the metal concentration may be due to covering /coating of the most surface sites of Fe$_3$O$_4$-PPCQDs with high concentration of Pb(II) and Cd(II) and the adsorption capacity of the adsorbent get exhausted due to non-availability of free binding sites [25]. Also, at low concentration ranges, the percentage of adsorption is high because of the availability of more active sites on the surface of adsorbent. Figure 10b showed that the adsorption capacity against ion concentrations. The increase in adsorption capacity depended on initial metal concentration which was led to increase the diffusion of Pb(II) and Cd(II) ions from the liquid phase to the surface of the solid phase. So, the driving force of the metal ions cause to lead to the collisions between metal ions and the nanoparticles surface. Therefore, the adsorption capacity was increased [23].

### 3.7. Adsorption thermodynamic

The adsorption process was analyzed by thermodynamic theory. The thermodynamic parameters viz. standard Gibb's free energy ($\Delta G°$), standard enthalpy ($\Delta H°$) and standard entropy ($\Delta S°$) for the removal of Pb(II) and Cd(II) by the Fe$_3$O$_4$-PPCQDs were calculated by Equations 2-5 [26]:

$$\Delta G° = -RT \ \ln \ K \qquad \text{(Eq. 2)}$$

$$\Delta H^0 = \left[\frac{RT_1 T_2}{(T_2 - T_1)}\right] \ln\left(\frac{K_2}{K_1}\right) \qquad \text{(Eq. 3)}$$

$$\Delta S^0 = \left(\frac{\Delta H^0 - \Delta G^0}{T}\right) \qquad \text{(Eq. 4)}$$

$$K = \left(\frac{qe}{Ce}\right) \qquad \text{(Eq. 5)}$$

where R (8.314 J mol$^{-1}$ K$^{-1}$) is the universal gas constant, K is the equilibrium constant at temperature T, T is the absolute temperature (K), Ce (mg L$^{-1}$) is the equilibrium concentration and qe is the amount of Cd(II) and Pb(II) adsorbed on the surface of the Fe$_3$O$_4$-PPCQDs. Figure 11 shows the relationship between $\Delta G°$ and temperature. Table 1 gives the thermodynamic parameters for adsorption of Cd(II) and Pb(II) adsorbed on the surface of the Fe$_3$O$_4$-PPCQDs adsorbent at different temperatures. As can be seen from the Table 1 the negative value of $\Delta G°$ signifies that the adsorption process is feasible and spontaneous in nature. With the increase in temperature, $\Delta G°$ shifts to more positive values indicating that the increase in temperature

was not favorable for the adsorption process [27]. The negative value of ΔH° signifies that the adsorption process is exothermic. That was also the reason equilibrium adsorption of Cd(II) and Pb(II) decreased as the rising of solution temperature (Effect of temperature). The value of ΔS were −20.31 and −6.38 J mol⁻¹ K⁻¹ for adsorption of Cd(II) and Pb(II) ions, which reflected that the randomness at the interface of the $Fe_3O_4$-PpCQDs and solution was reduced during the adsorption process.
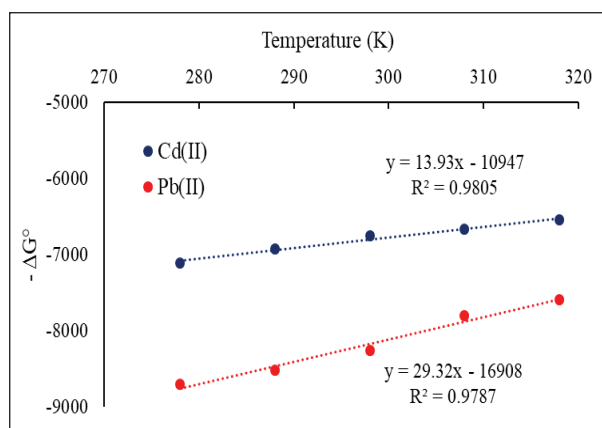


**Fig.11**. Relationship between ΔG° and temperature

### 3.8. Adsorption isotherms

The most popular isotherms are Langmuir and Freundlich [28] models. The Langmuir model describes monolayer adsorption, however Freundlich model show heterogeneous surface. The linear form of Langmuir model is given by following Equation 6:

$$\frac{C_e}{q_e} = \frac{1}{(K_L q_m)} + \frac{C_e}{q_m} \qquad \text{(Eq. 6)}$$

where $C_e$ (mg L⁻¹) is the equilibrium concentration of the solution, $q_e$ (mg g⁻¹) is the amount of metal adsorbed per specific amount of adsorbent, $q_m$ (mg g⁻¹) is the maximum amount of metal ions required to form monolayer, K (L mg⁻¹) is the adsorption equilibrium constant (Fig. 12). Freundlich adsorption model demonstrate that adsorbents have a heterogeneous surface having site with different adsorption potential. It moreover expects that stronger binding sites are occupied first and the binding strength decreases with the increasing degree of occupation. The Freundlich adsorption model in its linear form is given in Equation 7:

$$\log_{10} q_e = \log_{10}(K_f) + \left(\frac{1}{n}\right)\log_{10}(C_e) \quad \text{(Eq. 7)}$$

where $K_f$ (mg g⁻¹) is the Freundlich constant indicating adsorption capacity, n (L mg⁻¹) is the adsorption intensity that is the measure of the change in affinity of the adsorbate with the change in adsorption density. The Freundlich constants $K_f$ and n were calculated from the slope and intercept of the plot of Ce versus log10 qe (Fig. 13) that shown in Table 2. The values of Langmuir R² for Cd(II) and Pb(II) by the $Fe_3O_4$-PPCQDs were higher than Freundlich model thus, indicating that Langmuir model fitted the data in good congruence, thereby indicating monolayer adsorption.

**Table 1.** Thermodynamic parameters for adsorption of Pb(II) and Cd(II) by $Fe_3O_4$-PPCQDs at different temperatures

| Ion | T (K) | ΔG (J mol⁻¹) | ΔH (J mol⁻¹) | ΔS (J mol⁻¹) | R² |
|---|---|---|---|---|---|
| Pb (II) | 278 | -8700 | -16908 | -29.32 | 0.978 |
| | 288 | -8510 | | | |
| | 298 | -8256 | | | |
| | 308 | -7800 | | | |
| | 318 | -7589 | | | |
| Cd (II) | 278 | -7105 | -10947 | -13.93 | 0.980 |
| | 288 | -6923 | | | |
| | 298 | -6748 | | | |
| | 308 | -6664 | | | |
| | 318 | -6538 | | | |
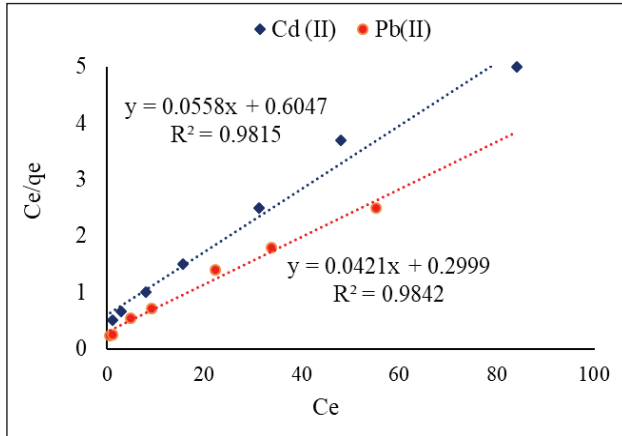
**Fig. 12.** Linear Langmuir isotherm for Pb(II) and Cd(II) removal by the Fe$_3$O$_4$-PPCQDs.
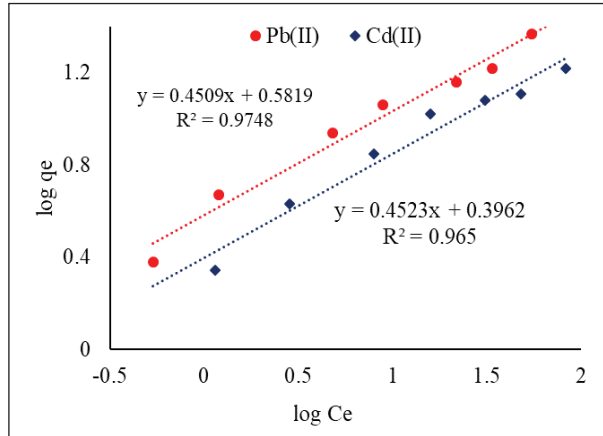


**Fig. 13.** Linear Freundlich isotherm for Pb(II) and Cd(II) removal by the Fe$_3$O$_4$-PPCQDs.

**Table 2.** Langmuir and Freundlich isotherm parameters for the removal of Pb(II) and Cd(II) by the Fe$_3$O$_4$-PPCQDs

| Parameters | Pb(II) | Cd(II) |
|---|---|---|
| *Langmuir parameters* | | |
| $q_m$ (mg g$^{-1}$) | 23.75 | 17.92 |
| b (L mg$^{-1}$) | 0.120 | 0.092 |
| $R^2$ | 0.9842 | 0.9815 |
| *Freundlich Parameters* | | |
| $K_f$ (mg g$^{-1}$) | 3.82 | 2.5 |
| n (L mg$^{-1}$) | 2.22 | 2.21 |
| $R^2$ | 0.9748 | 0.965 |

### 3.9. Comparison of adsorption capacity with other adsorbents

The maximum adsorption capacity of Fe$_3$O$_4$-PPCQDs nanocomposite for the removal of Pb(II) and Cd(II) was compared with other adsorbents reported in the literature and the values are given in Table 3. It is clear from Table 3, that the adsorption capacity of Fe$_3$O$_4$-PPCQDs. is comparable with other nanomaterials suggesting that, it is effective in removing Pb(II) and Cd(II) from aqueous solutions [29-33].

**Table 3.** Comparison of adsorption capacity of the Fe$_3$O$_4$-PPCQDs with other adsorbents.

| Adsorbents | Adsorption capacity (mg g$^{-1}$) | | pH | Adsorbent mass (mg). | Ref. |
|---|---|---|---|---|---|
| | Cd (II) | Pb (II) | | | |
| CFe$_3$O$_4$ | 4.106 | 3.795 | 3 | 50 | 29 |
| PMNPs | 29.60 | 3.103 | 1 to 8 | 50 | 30 |
| Kaniar Fe$_3$O$_4$ | 2.20 | 1.35 | 5 | 200 | 31 |
| MCANF | ----- | 44 | 6 | 100 | 32 |
| Sawdust (Fe3O4/SC) | 63 | ----- | 6.5 | 400 | 33 |
| This study | 17.92 | 23.75 | 6 | 100 | ----- |

CFe$_3$O$_4$: Chitosan/iron oxide nanocomposite
PMNPs: Polymer-modified magnetic nanoparticles
Kaniar Fe$_3$O$_4$: Magnetic Bauhinia purpurea (Kaniar) powders
MCANF: Fe$_3$O$_4$ nanoparticles onto cellulose acetate nanofibers nanocomposite

## 4. Conclusions

In this article, the adsorption potential of the $Fe_3O_4$-PPCQDs nanocomposite was investigated for the removal of Pb(II) and Cd(II) ions. TEM analysis revealed that the synthesized nanoparticles have an average particle size of 10-25 nm for the $Fe_3O_4$-PPCQDs. The XRD analysis of $Fe_3O_4$-PPCQDs confirmed the presence of magnetite phase exhibiting average crystal size similar to that indicated by the TEM analysis. Batch adsorption experiments were led to study the effect of various parameters like agitation time, adsorbent dosage, initial concentration of the Pb(II) and Cd(II), temperature, and pH. The conditions for the highest removal efficiency of synthesized nanocomposite for the removal of Pb(II) and Cd(II) were achieved (pH=6.0, temperature=25 ±1°C, initial metal ion concentration=50 mg $L^{-1}$ contact time =20 min). Based on procedure, the maximum Langmuir adsorption capacity was obtained 17.92 mg $g^{-1}$ for Cd(II) and 23.75 mg $g^{-1}$ for Pb(II) at pH 6. In addition, the working ranges of cadmium and lead adsorption based on $Fe_3O_4$-PPCQDs nanocomposite in 50 mL of water samples were obtained 4-36 µg $L^{-1}$ and 50-400 µg $L^{-1}$, respectively by the MSPE procedure (PF=50, RSD%<2.4). Therefore, the ultra- trace analysis of Pb(II) and Cd(II) ions was done by $Fe_3O_4$-PPCQDs nanocomposite at pH=6.

## 5. Acknowledgments

## 6. References

[1]    A. T. Jan, M. Azam, K. Siddiqui, A.A.I. Choi, Q.M.R. Haq, Heavy metals and human health: mechanistic insight into toxicity and counter defense system of antioxidants. Int. J. Mol. Sci., 16 (2015) 29592–29630.

[2]    R. Singh, N. Gautam, A. Mishra, R. Gupta, Heavy metals and living systems: an overview. Indian J. Pharmacol., 43 (2011) 246-253.

[3]    W. Shotyk, G.L. Roux, A. Sigel, H. Sigel, R.K.O. Sigel, Metal ions in biological systems, Taylor and Francis, Boca Raton, Chapter 10, 2005.

[4]    M.A.A. Zaini, R. Okayama, M. Machida, Adsorption of aqueous metal ions on cattle-manure compost based activated carbons, J. Hazard. Mater., 170 (2009) 1119-1124.

[5]    A. Vázquez-Guerrero, R. Cortés-Martínez, R. A. Cuevas-Villanueva, E. M. Rivera-Muñoz, R. Huirache-Acuña, Cd(II) and Pb(II) adsorption using a composite obtained from Moringa oleifera Lam, cellulose nanofibrils impregnated with iron nanoparticles, Water, 13 (2021) 89.

[6]    W. Zhang, X. Shi, Y. Zhang, W. Gu, B. Li, Synthesis of water-soluble magnetic graphene nanocomposites for recyclable removal of heavy metal ions, J. Mater. Chem. A, 1 (2013) 1745-1753.

[7]    H. Isawi, Using zeolite/polyvinyl alcohol/ sodium alginate nanocomposite beads for removal of some heavy metals from wastewater, Arab. J. Chem., 13 (2020) 5691-5716.

[8]    R. Ahmad, A. Mirza, Facile one pot green synthesis of chitosan-iron oxide ($CS-Fe_2O_3$) nanocomposite: removal of Pb(II) and Cd(II) from synthetic and industrial wastewater, J. Clean. Prod., 186 (2018) 342-352.

[9]    H. C. Tao, H. R. Zhang, J. B. Li, W. Y. Ding, Biomass based activated carbon obtained from sludge and sugarcane bagasse for removing lead ion from wastewater, Bioresour. Technol., 192 (2015) 611-617.

[10]  M. F. Gao, Q. L. Ma, Q.W. Lin, J. L. Chang, H. Z. Ma, A novel approach to extract $SiO_2$ from fly ash and its considerable adsorption properties, Mater. Design., 116 (2017) 666–675.

[11]  Y. K. Tang, L. Chen, X. R. Wei, Q. Y. Yao, T. Li, Removal of lead ions from aqueous solution by the dried aquatic plant, Lemna perpusilla Torr, J. Hazard. Mater., 244 (2013) 603-612.

[12] J. G. Wang, J. Wei, J. Li, Rice straw modified by click reaction for selective extraction of noble metal ions, Bioresour. Technol., 177 (2015) 182-187.

[13] T. M. Abdel-Fattah, M. E. Mahmoud, S. B. Ahmed. Biochar from woody biomass for removing metal contaminants and carbon sequestration, J. Ind. Eng. Chem., 22 (2015) 103-109.

[14] S. Haider, F.A.A. Ali, A. Haider, W. A. Al-Masry, Y. Al-Zeghayer, Novel route for amine grafting to chitosan electrospun nanofibers membrane for the removal of copper and lead ions from aqueous medium, Carbohydr. Polym., 199 (2018) 406-414.

[15] Q. Feng, D. Wu, Y. Zhao, A. Wei, Q. Wei, H. Fong, Electrospun AOPAN/RC blend nanofiber membrane for efficient removal of heavy metal ions from water, J. Hazard. Mater., 344 (2018) 819–828.

[16] Q. Lv, X. Hu, X. Zhang, L. Huang, Z. Liu, G. Sun, Highly efficient removal of trace metal ions by using poly (acrylic acid) hydrogel adsorbent, Mater. Design., 181 (2019) 107934.

[17] F. Arshad, M. Selvaraj, J. Zain, F. Banat, M. Abu Haija, Polyethylenimine modified graphene oxide hydrogel composite as an efficient adsorbent for heavy metal ions, Sep. Purif. Technol., 209 (2019) 870-880.

[18] R. Song, M. Murphy, C. Li, K. Ting, C. Soo, Z. Zheng, Current development of biodegradable polymeric materials for biomedical applications, Drug Des. Devel. Ther., 24 (2018) 3117-3145.

[19] H. Baweja, K. Jeet, Economical and green synthesis of graphene and carbon quantum dots from agricultural waste, Mater. Res. Express, 6 (2019) 0850g8.

[20] M. M. Rhaman, M. R. Karim, M. K. Mohammad Ziaul, Y. Ahmed, Removal of chromium (VI) from effluent by a magnetic bioadsorbent based on Jute Stick powder and its adsorption isotherm, kinetics and regeneration study, Water Air Soil Pollut.,

231 (2020) 1-18.

[21] P.N. Dave, L.V. Chopda, Application of iron oxide nanomaterials for the removal of heavy metals, J. Nanotechnol., 4 (2014) 1-14

[22] M.O. Ojemaye, O.O. Okoh, A.I. Okoh, Surface modified magnetic nanoparticles as efficient adsorbents for heavy metal removal from wastewater, progress and prospects, Mater. Express, 7 (2017) 439-456.

[23] B. R. Seeram, M. Lee, D. Heber, Rabid large scale purification of ellagitunnins from pomegranate husk, Sep. Puri. Technol., 41 (2005) 49-55.

[24] H. Wang, X. Xu, Z. Ren, B. Gao, Removal of phosphate and chromium(VI) from liquids by an aminecrosslinked nano-Fe$_3$O$_4$ biosorbent derived from corn straw, RSC Adv., 6 (2016) 47237-47248.

[25] M. Jain, M Yadav, T. Kohout, M. Lahtinen, V.K. Garg, Development of iron oxide/ activated carbon nanoparticle composite for the removal of Cr(VI), Cu(II) and Cd(II) ions from aqueous solution, Water Resour. Ind., 20 (2018) 54-74

[26] M.I. Panayotova, Kinetics and thermodynamics of copper ions removal from wastewater by use of zeolite, Waste Manag., 21 (2001) 671-676.

[27] L. Xu, X. Zheng, H. Cui, Z. Zhu, J. Liang, J. Zhou, Equilibrium, kinetic, and thermodynamic studies on the adsorption of cadmium from aqueous solution by modified biomass ash, Bioinorg. Chem. Appl., 2017 (2017) 1-9. https://doi.org/10.1155/2017/3695604

[28] H. Zare, H. Heydarzadeh, M. Rahimnejad, A. Tardast, M. Seyfi, S.M. Peyghambarzade, Dried activated sludge as an appropriate biosorbent for removal of copper (II) ions, Arab. J. Chem., 8 (2015) 858-864.

[29] M. Keshvardoostchokami, L. Babaei, A. A. Zamani, A. H. Parizanganeh, F. Piri, Synthesized chitosan/iron oxide nanocomposite and shrimp shell in removal

of nickel, cadmium and lead from aqueous solution, Global J. Environ. Sci. Manag., 3 (2017) 267–278.

[30] F. Ge, M. Li, H. Ye, B. Zhao, Effective removal of heavy metal ions $Cd^{2+}$, $Zn^{2+}$, $Pb2+$, $Cu^{2+}$ from aqueous solution by polymer-modified magnetic nanoparticles, J. Hazard. Mater., 211 (2012) 366–372.

[31] R. Sharma, A. Sarswat, C.U. Pittman, D. Mohan, Cadmium and lead remediation using magnetic and non-magnetic sustainable biosorbents derived from bauhinia Purpurea Pods, RSC Adv., 7 (2017) 8606–8624.

[32] T. I. Shalaby, M.F. El-Kady, A.E.H.M. Zaki, S. M. El-Kholy. Preparation and application of magnetite nanoparticles immobilized on cellulose acetate nanofibers for lead removal from polluted water, Water Supply, 17 (2017) 176–187.

[33] N. Kataria, V. K. Garg, Green synthesis of $Fe_3O_4$ nanoparticles loaded sawdust carbon for cadmium (II) removal from water: regeneration and mechanism, Chemosphere, 208 (2018) 818–828.